Available online at BCREC Website: https://bcrec.undip.ac.id

Bulletin of Chemical Reaction Engineering & Catalysis, 14 (2) 2019, 336-344

Research Article

Solid-phase Synthesis of Visible-light-driven $BiVO_4$ Photocatalyst and Photocatalytic Reduction of Aqueous Cr(VI)

Jing Li[1,*], Yan Chen[1], Chengru Chen[2], Shaorong Wang[3]

[1]School of Chemistry and Chemical Engineering, Xuzhou University of Technology, 221111, Xuzhou, China
[2]School of Mechanical & Electrical Engineering, Xuzhou University of Technology, 221111, Xuzhou, China
[3]School of Chemical Engineering and Technology, China University of Mining and Technology, 221111, Xuzhou, China

Received: 9th September 2018; Revised: 16th January 2019; Accepted: 23th January 2019; Available online: 30th April 2019; Published regularly: 1st August 2019

Abstract

This communication reports a pioneering study on the synthesis of $BiVO_4$ and photocatalytic reduction of Cr(VI)-polluted wastewaters. Monoclinic phase $BiVO_4$ micron-crystals with adjustable morphology were synthesized via a solid-phase route. The structures, morphology, optical properties of the $BiVO_4$ micron-crystals were characterized by X-ray diffraction, field emission scanning electron microscopy, UV-vis diffuse reflectance spectra, Fourier transform infrared spectroscopy spectra, and photocurrent measurements. Besides, their photocatalytic properties were tested for the reduction of aqueous Cr(VI) under visible light ($\lambda > 420$ nm) irradiation. The photocatalytic tests showed that the photocatalytic activities of $BiVO_4$ powders in aqueous Cr(VI) depended on the dark adsorption amount for Cr(VI) and number of photogenerated carriers. $BiVO_4$-(c) exhibited the highest photocatalytic reduction efficiency that attributed to highest separation and transfer efficiency of photogenerated electrons and holes. Besides, effects of photocatalytic experiment parameters (including dosage of photocatalyst and coexistent anions and cations) on the Cr(VI) removal rate by $BiVO_4$-(c) were also investigated, and $\cdot OH$ play an important role in the $BiVO_4$ photocatalytic reduction Cr(VI).

Keywords: Semiconductors; Photocatalysis; Visible-light Driven; Hexavalent Chromium Reduction

How to Cite: Li, J., Chen, Y., Chen, C., Wang, S. (2019). Solid-phase Synthesis of Visible-light-driven $BiVO_4$ Photocatalyst and Photocatalytic Reduction of Aqueous Cr(VI). *Bulletin of Chemical Reaction Engineering & Catalysis*, 14 (2): 336-344 (doi:10.9767/bcrec.14.2.3182.336-344)

Permalink/DOI: https://doi.org/10.9767/bcrec.14.2.3182.336-344

1. Introduction

Hexavalent chromium (Cr(VI)) is a common heavy metal contaminant in the effluents from chromate-related industries, such as electroplating, pigment production, leather tanning [1-4]. Cr(VI) has acute toxicity and high mobility in water, which induced multiple human diseases and ecological problems [4-6], also the world health organization proposed the concentration of Cr(VI) in drinking water should be less than 0.05 mg/L. Therefore, it is urgently develop eco-

* Corresponding Author.
E-mail: lijingxz111@163.com (J. Li)
Telp: +86 1595068952; Fax: +86 0516-85608300

nomical and environmental-friendly methods of removing the Cr(VI) wastewaters. Photocatalytic reduction of Cr(VI) into Cr(III) has now been proven as an effective procedure for treating Cr(VI) wastewaters [7-12] due to its high efficiency, low cost, environmental friendly, and exploitation of solar energy. Consequently, it is desirable to develop new visible-light-responsive semiconductor photocatalysts cater to industrial application of photocatalytic technology treat large scale Cr(VI) wastewaters, and make full use of solar energy.

Bismuth vanadate ($BiVO_4$) has attracted considerable attention due to its photocatalytic activity under visible light irradiation and higher stability [13-15]. $BiVO_4$ has three crystalline phase, respectively named as monoclinic scheelite, tetragonal zircon and tetragonal scheelite [13-15], of which the monoclinic bismuth vanadate with a band gap of 2.4 eV exhibits much higher visible-light photocatalytic activity [14]. It is well known that the photocatalytic properties strongly depend on the crystal structure [14,16], recently, monoclinic structure $BiVO_4$ powder was synthesized by various techniques, such as: Jiang [14] prepared spherical-shaped monoclinic structure $BiVO_4$ by the solution combustion synthesis method and improves the photocatalytic activity of degradation of methylene blue. Monoclinic bismuth vanadate powders were synthesized by aqueous processes and photodegradation of methylene blue solution was determined under visible-light irradiation (λ > 420 nm) [17]. $BiVO_4$ crystallites was prepared in the low-temperature molten salt method and exhibited UV-vis absorption [18]. Zhang [19] synthesized monoclinic structured $BiVO_4$ nanosheets in the presence of sodium dodecyl benzene sulfonate (SDBS) as a morphology-directing template by hydrothermal synthesis, also photodegradation of RB under solar irradiation. Zhou [20] obtained monoclinic scheelite structure $BiVO_4$ via sonochemical method, and the photocatalytic activities were also evaluated by decolorization of methyl orange under visible light. Zhang [21] reported that visible-light-driven $BiVO_4$ was synthesized by metalorganic decomposition method, and evaluated the photodegradation of MB. Although $BiVO_4$ as a visible light photocatalyst is used removing the organic pollution, there is rare report that $BiVO_4$ photocatalytic reduction of aqueous Cr(VI) under the visible light irradiation.

Herein, we report a simple synthesis of monoclinic $BiVO_4$ powders and photocatalytic activities of the as-synthesized $BiVO_4$ powders were evaluated in the reduction of aqueous Cr(VI) under visible-light (λ > 420 nm) irradiation. The effects of the coexistent anions and cations on Cr(VI) removal rate were analysed. Furthermore, reaction mechanism of photocatalytic reduction of hexavalent chromium by bismuth vanadate is proposed.

2. Materials and Methods

All the analytically grade reagents were used without further purification, and purchased from Sinopharm Chemical Reagent Co., Ltd. Water used in experiment was distilled and deionized.

2.1 Preparation of $BiVO_4$

The powders of 4.0 mmol of $Bi(NO_3)_3{\cdot}5H_2O$ and 4.0 mmol NH_4VO_3 were mixed in an agate mortar for 40 min, then the bronzing mixture were transferred into a corundum crucible at 300~700 °C for 2 h in a muffle furnace. After the crucible naturally cooled to room temperature, the resultant product was washed with deionized water and ethanol, and dried in air at 100 ºC for 5 h. For the convenience of description, the products obtained at the 300 ~ 700 °C were named $BiVO_4$-(a)~(e).

2.2 Material Characterization

X-ray diffraction (XRD) patterns were acquired using a German Bruker AXS D8 ADVANCE X-ray diffractometer. Field emission scanning electron microscope (FESEM) images were obtained using a Japan Hitachi S-4800 field emission scanning electron microscopy. Fourier transform infrared spectra were measured on German Bruker fourier transform infrared spectrometer at room temperature with the sample in a KBr beam splitter. UV-vis diffuse reflectance absorbance spectra were obtained on American Varian Cary 5000 UV-vis-NIR spectrophotometer with an integrating sphere attachment, employing $BaSO_4$ as reference. Photocurrent were obtained using a CHI660E electrochemical workstation, employing a conventional three-electrode electrochemical cell. The electrolyte solution was 0.1 mol/L Na_2SO_4 aqueous solution. The light source was a 35 W LED lamp for the photocurrent measurement.

2.3 Visible Light Photocatalytic Activity Studies

The photocatalytic activity of the as-synthesized samples was evaluated in the reduction of aqueous Cr(VI) under a 200 W Xe lamp (using cutoff filters) irradiation in photo-

chemical reactor. The experiments were performed at 25 ºC as follows: 100 ~ 500 mg photocatalyst powders and 1.0 mL of 100 mg/mL citric acid aqueous solution were added into quratz bottles with 300 mL of 30 mg/L $K_2Cr_2O_7$ aqueous solution, magnetically stirred in the dark for 80 min to realize Cr(VI) adsorption equilibrium. During the visible light (λ > 420 nm) irradiation, about 3 mL of suspension was taken out from the reactor at a fixed interval and filtered using cellulose acetate membrane filter with pore size is 0.22 μm to separate the photocatalyst powders. The Cr(VI) content in the filtrates was determined using the standard diphenylcarbazide method with a detection limit of 0.005 mg/L by measuring the absorbance at 540 nm [22].

3. Results and Discussion

3.1 Characterization of Samples

Crystalline structure and phase purity of the synthesized $BiVO_4$ samples were investigated by XRD. Figure 1 (a)~(e) show the XRD pattern of the as-synthesized $BiVO_4$, which prepared via the mixed powders of 4.0 mmol of $Bi(NO_3)_3{\cdot}5H_2O$ and 4.0 mmol NH_4VO_3 at 300 ~ 700 ºC for 2 h, respectively. All the XRD peaks of the as-prepared $BiVO_4$ exhibited well crystallinity, and showed an excellent match with JCPDS NO.14-0688 which represents monoclinic phase $BiVO_4$. Other diffraction peaks arising from possible impurities were not detected. The intensity of the diffraction peaks of $BiVO_4$ was stronger accordingly with increase of temperature.

It is known that the morphologies of the products are depend upon the intrinsic structure, and also relate to the growth kinetics of the reaction process. As can be seen from Figure 2, $BiVO_4$-(a), (b), (c), (d), and (e) are comprised micron-lever particles and exhibited different morphologies. The FESEM images of

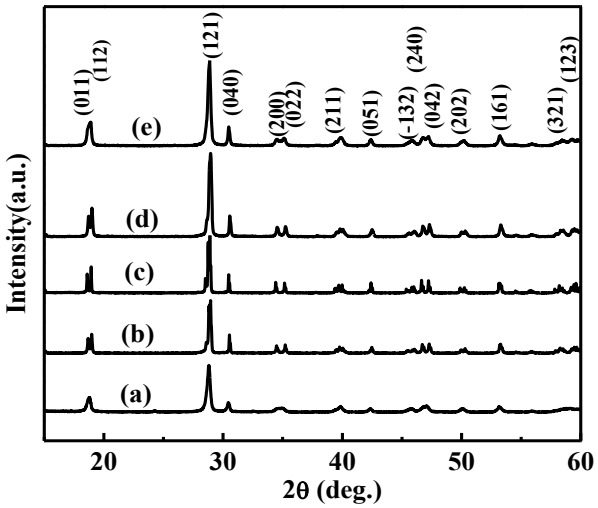

Figure 1. XRD patterns of as-synthesized $BiVO_4$-(a)~(e)

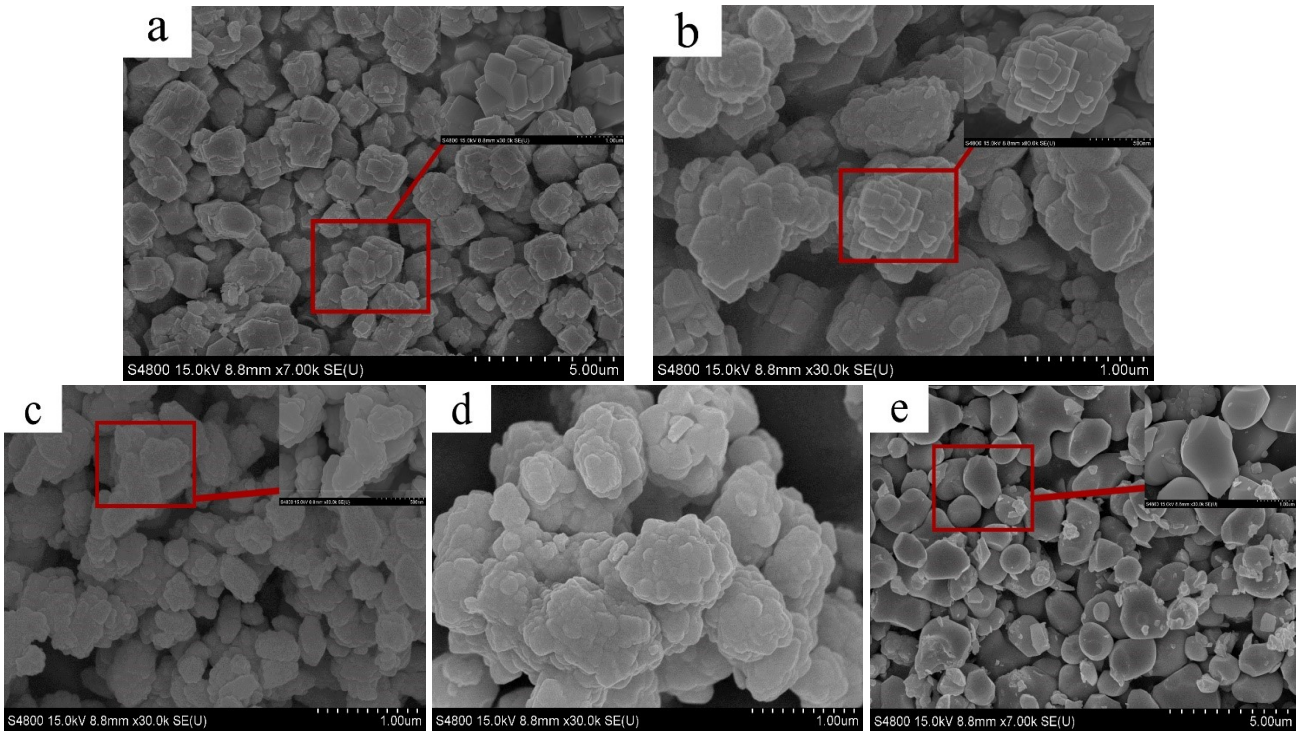

Figure 2. FESEM images of as-synthesized $BiVO_4$- (a)~(e)

$BiVO_4$-(a) and (b) showed a block-like accumulation structure (about 1~2 μm in size), which were combined of 120~160 nm blocks. With increasing the reaction temperature, the block-like nanoparticles transformed into nanoparticles and displayed serious agglomeration [3] which showed in Figure 2(c) and (d). It was seen that the smooth surface and irregular-shaped particles with 1~2 μm in Figure 2(e). The agglomeration phenomenon attributed to the faster speed of molecular movement led to the faster growth rate of the crystal nucleus when reaction temperature was increased, which formed the larger size particles [3,23,24]. The FESEM images disclosed the influence of reaction temperature on the size and morphology.

3.2 Optical Properties

FTIR spectra were further used to analyse the functional groups on $BiVO_4$-(a)~$BiVO_4$-(e) prepared by solid-state process (Figure 3). For the all sample of $BiVO_4$ powders exists a broad peak at 700~850 cm^{-1} with shoulders at 730, 830 cm^{-1}, furthermore a weak infrared band at 473 cm^{-1} is also visible. According the literature [24,25], Bi–O vibration is recorded at 473 cm^{-1}, 730 cm^{-1}, and 830 cm^{-1} assigned to the symmetric and asymmetric stretching vibration of the V–O, respectively. FTIR peaks at about 1637 cm^{-1} and 1382 cm^{-1}, which can be assigned to bending vibrations of absorbed H_2O molecules and absorbed NO_3^- [26], also the weaker infrared band of NO_3^- was observed at a higher temperature sample due to the desorption.

The photo-absorption abilities of the samples were measured by the UV-vis diffuse reflectance spectra according to the molecular spectra formed in the process of electrons move up to higher energy levels when the semiconductor absorb energy. Figure 4 displays the UV-vis diffuse reflectance spectra of as-synthesized monoclinic-phase $BiVO_4$, it can be seen all samples exhibit excellent light absorption in the UV-vis light region and has an absorption edge at about 550 nm. The band gap energy (E_g) of $BiVO_4$ were evaluated using the following equation [27,28]:

$$\alpha h\nu = B\,(h\nu - E_g)^{n/2} \quad (1)$$

where α, h, ν, E_g, and B are the absorption coefficient, Planck's constant, light frequency, the bandgap energy and a constant related to the material, respectively. The n symbol is determined by the type of optical transition of the semiconductor, n=1 for a direct transition and n=4 for a indirect transition. According to the previous literature, $BiVO_4$ is a direct band gap semiconductor [29,30], and n value equal 1. As shown in Figure 4, the bandgap energy of the $BiVO_4$ can be estimated from the curve of $(Bh\nu)^2$ versus $(h\nu)$, by extrapolating the linear portion of the $(Bh\nu)^2$ versus $(h\nu)$ curves to absorbance equal zero. The E_g values of $BiVO_4$-(a)~(e) were estimated to be about 2.43, 2.42, 2.40, 2.40, and 2.45 eV, respectively.

3.3 Photocatalytic Activity

The photocatalytic activities of $BiVO_4$-(a)~(e) are evaluated using Cr(VI) as target under visible light irradiation shown in Figure 5, and the equilibrium between Cr(VI) and $BiVO_4$-(a)~(e) can be achieved after mixed for 80 min in the presence of citric acid. Figure 5 showed that all the as-synthesized $BiVO_4$ had

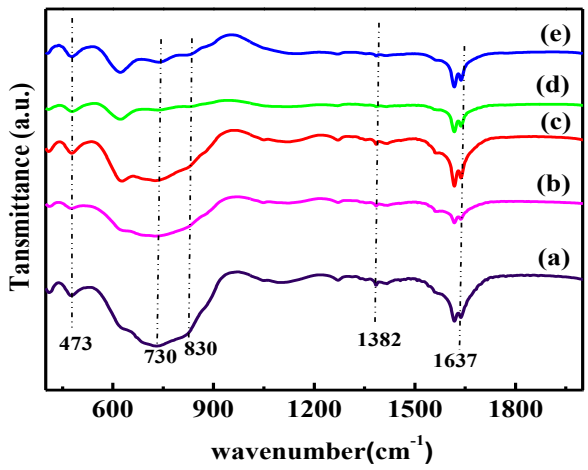

Figure 3. FTIR spectra of as-synthesized $BiVO_4$-(a)~(e)

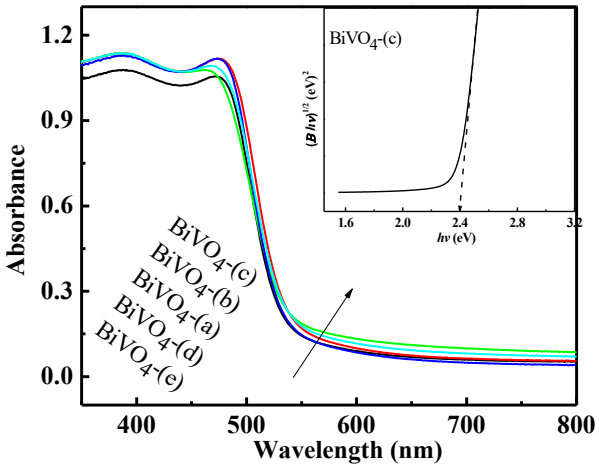

Figure 4. UV-vis diffuse reflectance spectra of $BiVO_4$- (a) ~(e) and plot of $(Bh\nu)^2$ versus $(h\nu)$ of $BiVO_4$- (c))

photocatalytic activities in the reduction of aqueous Cr(VI) under visible light irradiation, Cr(VI) concentration decreased continuously with increasing irradiation time. In contrast, both the photocatalytic activities and the dark adsorption amount for Cr(VI) of the as-synthesized $BiVO_4$ followed the same order of $BiVO_4$-(c) > $BiVO_4$-(b) > $BiVO_4$-(a) > $BiVO_4$-(d) > $BiVO_4$-(e) under the same visible light irradiation. For instance, the reduction rates of Cr(VI) over them were in turn 28.3 %, 24.2 %, 21.2 %, 15.7 % and 7.3 % after 100 min irradiation. The photocatalytic activities of $BiVO_4$-(a)~(e) differed greatly, indicating that the synthesis conditions of $BiVO_4$ played an important role in the process of photocatalysis.

The reaction rate constants (k) for photocatalytic reduction of Cr(VI) by different products were obtained using the pseudo-first order kinetic model [1,31-34]:

$$\ln(C_0/C_t) = kt \quad (2)$$

where C_0 and C_t denoted the Cr(VI) concentration at the irradiation time of 0 and t min, respectively. The plots of $\ln(C_0/C_t)$ vs irradiation time (t) as well as the obtained values of k and correlation coefficient (R^2) in the presence of different products are shown in Figure 6. It can be seen from Figure 6 that $BiVO_4$-(c) exhibited the highest visible light-driven photocatalytic activity, which was likely due to the most efficient separation and transfer of photogenerated electrons and holes (Figure 9). The E_g value of $BiVO_4$-(c) was estimated to be 2.40 eV which is the smallest band gap value among as-synthesized $BiVO_4$. Under the same intensity of visible light irradiation, $BiVO_4$-(c) can produce the most photogenerated carriers which also provides the most available photogenerated electrons for photocatalytic reduction of Cr(VI).

Figure 7 shows the photocatalytic activities of 100~500 mg $BiVO_4$-(c) and without photocatalyst in the reduction of aqueous Cr(VI) under visible light irradiation, also the contrast experiment (in present of photocatalyst and without light irradiation) was tested. As shown in Figure 7, the Cr(VI) concentration remained almost unchanged in the process of blank and contrast experiments, which disclosed that Cr(VI) can not undergo photodegradation when absent of $BiVO_4$. The dark adsorption amount for Cr(VI) is increasing as the dosages of $BiVO_4$-(c) increased, but he photocatalytic reduction rate of Cr(VI) increased firstly and then decreased. Furthermore 300 mg $BiVO_4$-(c) treated 300 mL of 30 mg/L $K_2Cr_2O_7$ exhibited

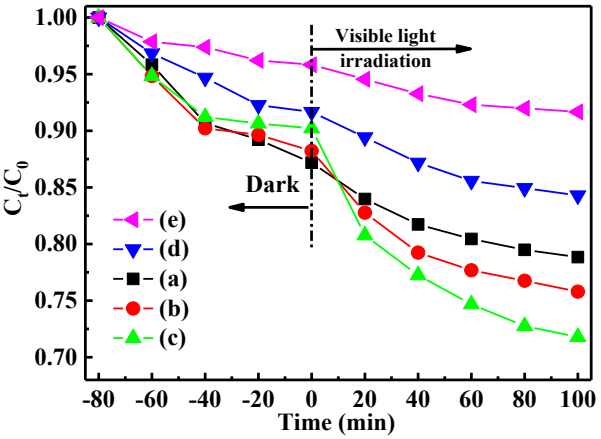

Figure 5. Photocatalytic reduction of aqueous Cr(VI) in the presence of $BiVO_4$-(a)~(e) under visible light irradiation

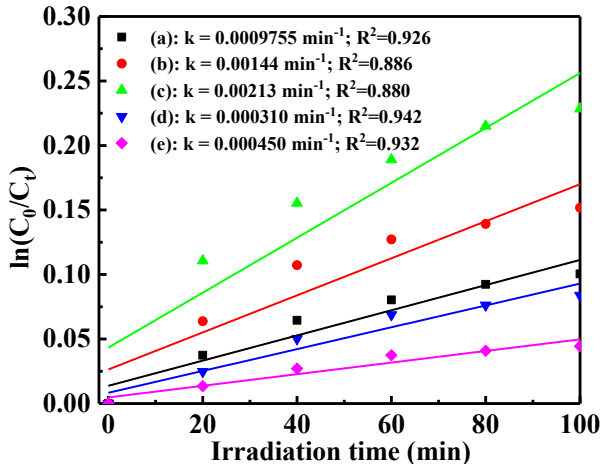

Figure 6. Plots of $\ln(C_0/C_t)$ vs irradiation time (t) for obtaining the values of reaction rate constant (k) and correlation coefficient (R^2) in the presence of different products

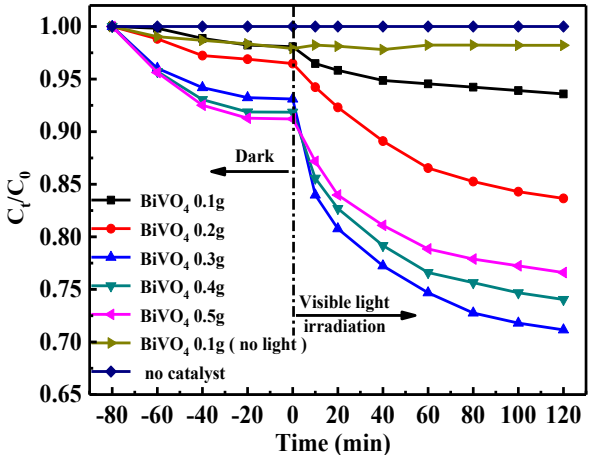

Figure 7. Photocatalytic reduction of aqueous Cr(VI) in the presence of different dosages of $BiVO_4$-(c) under visible light irradiation

the highest photocatalytic efficiency. The experimental results can be explained that the increase dosages of photocatalyst provided a large amount of surface-active points, but also increased suspension of solution [35].

The coexistent SO_4^{2-}, Cl^-, and NO_3^- anions as well as Mg^{2+} and Al^{3+} cations had no significant effects on the adsorption and photocatalytic reduction of Cr(VI) by $BiVO_4$-(c) (Figure 8). The coexistent PO_4^{3-} anions can obviously retard the photocatalytic reduction of Cr(VI) by $BiVO_4$-(c) (Figure 8), probably because that PO_4^{3-} can fiercely compete with Cr(VI) for the surface adsorption sites of the photocatalyst and H^+ ions in the solution [36]. In contrast, the coexistent Fe^{3+} and Cu^{2+} cations can greatly enhance the photocatalytic reduction of Cr(VI) by $BiVO_4$-(c) (Figure 8). It was possibly because that Fe^{3+} and Cu^{2+} may act as a catalyst or the media of electron transfer for the reduction of Cr(VI) [36,37], that is, photocatalytic reduction of Fe^{3+} and Cu^{2+} into Fe^{2+} and Cu^+ in the presence of organic acids (HCA) by $BiVO_4$-(c) can occur more easily, and the additional reduction of Cr(VI) by Fe^{2+} and Cu^+ can accelerate the total removal rate of Cr(VI).

4. Results and Discussions

The transient photocurrent responses of as-synthesized $BiVO_4$-(a)~(e) are shown in Figure 9. The photocurrent response was stability and regeneration in each switch-on and switch-off cycle for all $BiVO_4$-(a)~(e). Obviously, the photocurrents of $BiVO_4$-(c) were far larger than other, this remarkably increased photocurrent may be the result of faster electro transfer and a more efficient separation of photo-generated electrons and holes. Thus, $BiVO_4$-(c) were efficient in the generation, separation and transfer efficiency of photogenerated electrons and holes, which contributed to the greatly improved photocatalytic activity.

The valence band and conduction band edge positions of $BiVO_4$ was calculated from Equations (2) and (3) [27,38]:

$$E_{VB} = \chi - E_e + 0.5E_g \quad (2)$$

$$E_{CB} = E_{VB} - E_g \quad (3)$$

where χ is the energy of free electrons on the hydrogen scale, E_{VB}, E_{CB}, E_e, and E_g are the VB energy, CB energy, the absolute electronegativity with the value is 4.5 eV, and the band gap of the semiconductor, respectively. Therefore, χ is equal to 6.08 eV for $BiVO_4$, and the E_{VB} and E_{CB} value of $BiVO_4$ is calculated to be 2.78 eV and 0.38 eV.

Based on the calculation, the position of CB of $BiVO_4$ (+0.34 eV) is more positive than the potential of $O_2/\cdot O_2^-$ (−0.33 V *versus* NHE) [39], thus, the photoexcited electrons on the CB of pure $BiVO_4$ can not react with O_2 to produce $\cdot O_2^-$. However, the VB potential of $BiVO_4$ (2.74 eV) is higher than $\cdot OH/H_2O$ (+2.72 eV *versus* NHE) [40], so the holes in the VB of $BiVO_4$ can oxidize the absorbed water molecules to give more $\cdot OH$, another powerful active species for decomposing the chromophores of organic pollutant. As can be seen form Figure10, no ESR signals were observed when the reaction was performed in the dark. As expected the characteristic peak of $\cdot OH$ signals of $BiVO_4$, which implying the number of $\cdot OH$ radicals produced in the $BiVO_4$. Therefore, $\cdot OH$ play an important role in the $BiVO_4$ photocatalytic reduc-

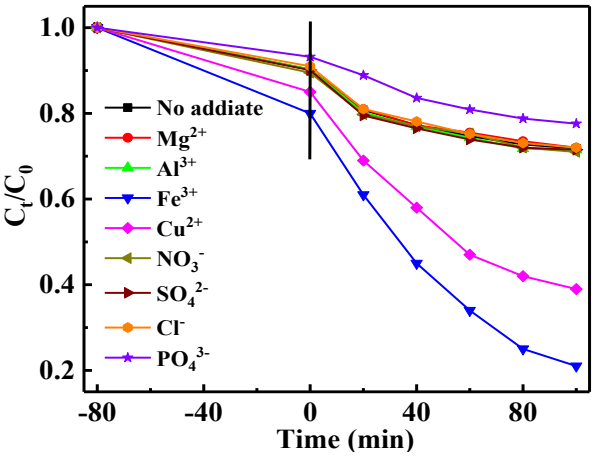

Figure 8. Effects of coexistent cations (sulfates) on the Cr(VI) removal rate by $BiVO_4$-(c)

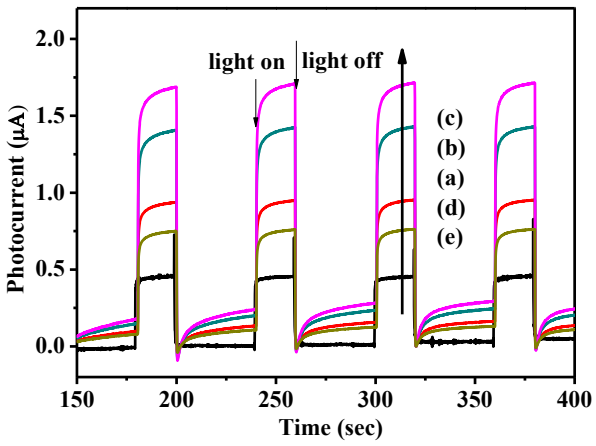

Figure 9. Transient photocurrent response of $BiVO_4$-(a)~(e) in 0.5 mol/L Na_2SO_4 under visible light illumination

tion Cr(VI). Based on the above analysis, a possible photocatalytic mechanism of $BiVO_4$ is proposed (Figure 11). Under the visible light irradiation, $BiVO_4$ can be initiated to yield the photogenerated electron-hole pairs. The photogenerated electrons on the CB edge of $BiVO_4$ cannot reduce O_2 into $\cdot O_2^-$ radicals, therefor Cr(VI) was reduced into Cr(III) by photogenerated electrons. At the same time, the holes in the VB of $BiVO_4$ could oxidize H_2O to yield $\cdot$OH, citric acid was used to scavenge the photogenerated holes, thus decreasing the recombination of electron-hole pairs and setting free more electrons available to reduce Cr(VI).

5. Conclusions

A high efficiency visible light-driven photocatalyst of monoclinic phase $BiVO_4$ was synthesized via solid-state technique. It was found that the influence of reaction temperature on the size and morphology. The as-synthesized $BiVO_4$ powders exhibit excellent visible light absorption and had photocatalytic activities in the reduction of aqueous Cr(VI) under visible light irradiation. The as-synthesized $BiVO_4$-(c) exhibited the highest photocatalytic reduction efficiency that attributed to much higher separation and transfer efficiency of photogenerated electrons and holes. The coexistent PO_4^{3-} anions can obviously retard the photocatalytic reduction of Cr(VI), and Fe^{3+}, and Cu^{2+} cations can greatly enhance the photocatalytic reduction of Cr(VI) by $BiVO_4$. The $\cdot$OH play an important role in the $BiVO_4$ photocatalytic reduction Cr(VI).

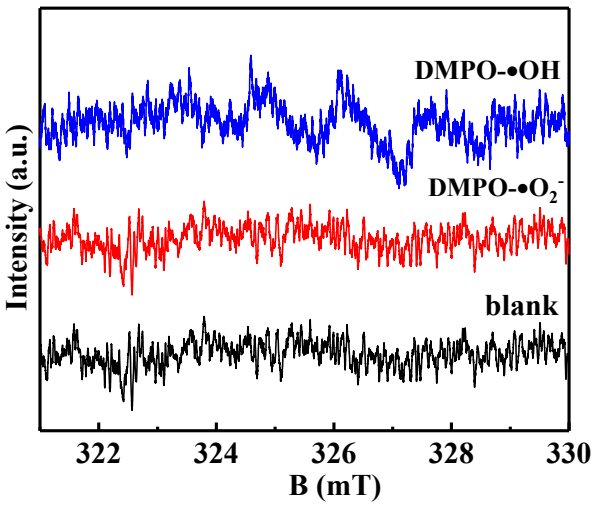

Figure 10. DMPO spin-trapping ESR spectra for $BiVO_4$-(C), in methanol dispersion for DMPO-$\cdot O_2^-$ and in aqueous dispersion for DMPO-$\cdot$OH

Acknowledgments

This research was financially supported by the Natural Science Foundation of Jiangsu Province (Grant NO. BK20171168), Science and Technology Project of Xuzhou (Grant NO. KC16SG246), Major Program of Natural Science Foundation of the Jiangsu Higher Education Institutions of China (Grant NO. 18KJA430015), Excellent Yong Teacher of "Blue Project" in Jiangu Province (2018).

References

[1] Lu, D.Z., Chai, W.Q. Yang, M.C., Fang, P.F., Wu, W.H., Zhao B., Xiong, R.Y., Wang, H.M. (2016). Visible Light Induced Photocatalytic Removal of Cr(VI) over TiO_2-based Nanosheets Loaded with Surface-enriched CoO_x Nanoparticles and Its Synergism with Phenol Oxidation. *Applied Catalysis B: Environmental*, 190: 44-65.

[2] Qiu, B., Xu, C.X., Sun, D.Z., Wei, H.G., Zhang, X., Guo, J., Wang, Q., Rutman, D., Guo, Z.H., Wei, S.Y. (2014). Polyaniline Coating on Carbon Fiber Fabrics for Improved Hexavalent Chromium Removal. *RSC Advances*, 4: 29855-29865.

[3] Zhang, Y.C., Li, J., Zhang, M., Dionysiou, D.D. (2011). Size-tunable Hydrothermal Synthesis of SnS_2 Nanocrystals with High Performance in Visible Light-driven Photocatalytic Reduction of Aqueous Cr(VI). *Environmental Science & Technology*, 45: 9324-9331.

[4] Wang, L., Li, X.Y., Teng, W., Zhao, Q.D., Shi, Y., Yue, R.L., Chen, Y.Y. (2013). Efficient Photocatalytic Reduction of Aqueous Cr(VI) over Flower-like $SnIn_4S_8$ Microspheres under Visible Light Illumination. *Journal of Hazardous Materials*, 244-245: 681-688.

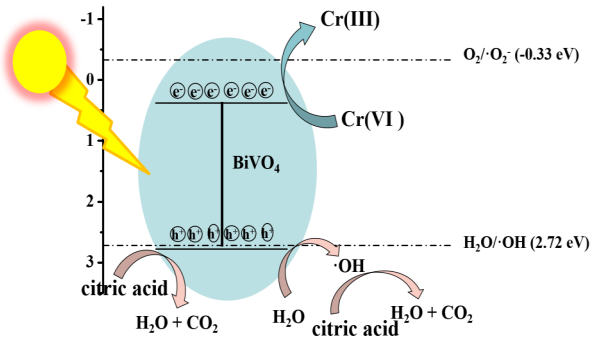

Figure 11. The possible photocatalytic mechanism of $BiVO_4$-(C) for reduction of Cr(VI) under visible light irradiation

[5] Kameda, T., Kondo, E., Yoshioka, T. (2014). Preparation of Mg-Al Layered Double Hydroxide Doped with Fe^{2+} and Its Application to Cr(VI) Removal. *Separation and Purification Technology*, 122: 12-16.

[6] Petala, E., Dimos, K., Douvalis, A., Bakas, T., Tucek, J., Zbořil, R., Karakassides, M.A. (2013). Nanoscale Zero-valent Iron Supported on Mesoporous Silica: Characterization and Reactivity for Cr(VI) Removal from Aqueous Solution. *Journal of Hazardous Materials*, 261: 295-306.

[7] Li, N., Tian, Y., Zhao, J.H., Zhang, J., Zhang, J., Zuo, W., Ding, Y. (2017). Efficient Removal of Chromium from Water by Mn_3O_4@ZnO/Mn_3O_4 Composite under Simulated Sunlight Irradiation: Synergy of Photocatalytic Reduction and Adsorption. *Applied Catalysis B: Environmental*, 214: 126-136.

[8] Liu, Y., Liu, S., Wu, T., Lin, H., Zhang, X. (2017). Facile Preparation of Flower-like Bi_2WO_6/CdS Heterostructured Photocatalyst with Enhanced Visible-light-driven Photocatalytic Activity for Cr(VI) Reduction. *Journal Sol-Gel Science and Technology*, 83(2): 315-323.

[9] Yang, W., Liu, Y., Hu, Y., Zhou, M., Qian, H. (2012). Microwave-assisted Synthesis Of Porous CdO-CdS Core-shell Nanoboxes with Enhanced Visible-light-driven Photocatalytic Reduction of Cr(VI). *Journal of Materials Chemistry*, 22(28): 13895-13898.

[10] Wang, H., Yuan, X., Wu, Y., Zeng, G., Chen, X., Leng, L., Wu, Z., Jiang, L., Lie, H. (2015). Facile Synthesis of Amino-Functionalized Titanium Metal-organic Frameworks and their Superior Visible-light Photocatalytic Activity for Cr(VI) Reduction. *Journal of Hazardous Materials*, 286: 187-194.

[11] Ji, W., Qu, J., Li, C.A., Wu, J.W., Jing. S., Gao, F., Lv, Y.N., Liu, C., Zhu, D.R., Ren, X.M., Huang, W. (2017). In Situ Surface Assembly of Core-shell TiO_2-copper(I) Cluster Nanocomposites for Visible-light Photocatalytic Reduction of Cr(VI), *Applied Catalysis B: Environmental*, 205: 368-375.

[12] Makama, A.B., Salmiaton1, A., Saion, Elias B., Choong, T.S.Y., Abdullah, N. (2017). Photocatalytic Reduction of Aqueous Cr(VI) with CdS under Visible Light Irradiation: Effect of Particle Size. *Bulletin of Chemical Reaction Engineering & Catalysis*, 12 (1): 62-70.

[13] Liu, W., Yu, Y.Q., Cao, L.X., Su, G., Liu, X.Y., Zhang, L., Wang, Y.G. (2010). Synthesis of Monoclinic Structured $BiVO_4$ Spindly Microtubes in Deep Eutectic Solvent and their Application for Dye Degradation. *Journal of Hazardous Materials*, 181(1): 1102-1108.

[14] Jiang, H.Q., Endo, H., Natori, H., Nagai, M., Kobayashi, K. (2008). Fabrication and Photoactivities of Spherical-shaped BiVO Photocatalysts through Solution Combustion Synthesis Method. *Journal of the European Ceramic Society*, 28(15): 2955-2962.

[15] Thalluri, S.M., Hussain, M., Saracco, G., Barber, J., Russo, N. (2014). Green-synthesized $BiVO_4$ Oriented Along {040} Facets for Visible-light-driven Ethylene Degradation. *Industrial & Engineering Chemistry Research*, 53(7): 2640-2646.

[16] Zhang, A., Zhang, J., Cui, N., Tie, X., An, Y. (2009). Effects of pH on Hydrothermal Synthesis and Characterization of Visible-light-driven $BiVO_4$ Photocatalyst. *Journal of Molecular Catalysis A Chemical*, 304(1): 28-32.

[17] Zhang, X., Ai, Z.H., Jia, F.L., Zhang, L.Z., Fan, X.X., Zou, Z.G. (2007). Selective Synthesis and Visible-light Photocatalytic Activities of $BiVO_4$ with Different Crystalline Phases. *Materials Chemistry Physics*, 103(1):162-167.

[18] Liu, Y., Ma, J.F., Liu, Z.S., Dai, C.H., Song, Z.W., Sun, Y., Fang, J. R., Zhao, J.G. (2010). Low-temperature Synthesis of BiVO Crystallites in Molten Salt Medium and their UV–vis Absorption. *Ceramics International*, 36(7): 2073-2077.

[19] Zhang, L., Chen, D.R., Jiao, X.L. (2006). Monoclinic Structured $BiVO_4$ Nanosheets: Hydrothermal Preparation, Formation Mechanism, and Coloristic and Photocatalytic Properties. *Journal of Physical Chemistry B*, 110(6): 2668-2673.

[20] Zhou, L., Wang, W.Z., Liu, S.W., Zhang, L.S., Xu, H.L., Zhu, W. (2006). A Sonochemical Route to Visible-light-driven High-activity $BiVO_4$ Photocatalyst. *Journal of Molecular Catalysis A: Chemical*, 252(1-2): 120-124.

[21] Zhang, J., Cui, H., Wang, B., Li, C., Zhai, J.P., Li, Q. (2013). Fly Ash Cenospheres Supported Visible-light-driven $BiVO_4$ Photocatalyst: Synthesis, Characterization and Photocatalytic Application. *Chemical Engineering Journal*, 223: 737-746.

[22] Li, J., Wang, T.X., Du, X.H. (2012). Preparation of Visible Light-driven SnS_2/TiO_2 Nanocomposite Photocatalyst for the Reduction of Aqueous Cr(VI). *Separation and Purification Technology*, 101(45): 11-17.

[23] Ju, P., Wang, P., Li, B., Fan, H., Ai, S., Zhang, D., Wang, Y. (2014). A Novel Calcined Bi_2WO_6/$BiVO_4$ Heterojunction Photocatalyst with Highly Enhanced Photocatalytic Activity. *Chemical Engineering Journal*, 236: 430-437.

[24] Zhang, L., Wang, H., Chen Z., Wong P., Liu J. (2011). Bi_2WO_6 Micro/nano-structures: Synthesis, Modifications and Visible-light-driven

Photocatalytic Applications. *Desalination and Water Treatment*, 106: 1-13.

[25] Dong, S.Y., Yu, C.F., Li, K.Y., Li, Y.H., Sun, J.H., Geng, X.F. (2014). Controlled Synthesis of T-shaped $BiVO_4$ and Enhanced Visible Light Responsive Photocatalytic Activity. *Journal of Solid State Chemistry*, 211(5): 176-183.

[26] Gotić, M., Musić, S., Ivanda, M., Šoufek, M., Popović, S. (2005). Synthesis and Characterization of Bismuth(III) Vanadate. *Journal of Molecular Structure*, 744: 535-540.

[27] Che. H., Liu, C., Hu, W., Hu, H., Li, J., Dou, J., Shi W, Li, C., Dong, H. (2018). NGQD Active Sites as Effective Collectors of Charge Carriers for Improving the Photocatalytic Performance of Z-scheme g-C_3N_4/Bi_2WO_6 Heterojunctions. *Catalysis Science & Technology*, 8: 622-631.

[28] Wang, Q., Guan, S. Y., Li, B. (2017). 2D Graphitic-C_3N_4 Hybridized with 1D Flux-grown Na-modified $K_2Ti_6O_{13}$ Nanobelts for Enhanced Simulated Sunlight and Visible-light Photocatalytic Performance. *Catalysis Science & Technology*, 7: 4064-4078.

[29] Ke, D.N., Peng, T.Y., Ma, L., Cai P., Dai K., (2009). Effects of Hydrothermal Temperature on the Microstructures of $BiVO_4$ and Its Photocatalytic O_2 Evolution Activity under Visible Light. *Inorganic Chemistry*, 48(11): 4685-4691.

[30] Chen, L., Yin, S.F., Huang, R., Zhang, Q., Luo S.L. (2012). Hollow Peanut-like m-$BiVO_4$: Facile Synthesis and Solar-Light-Induced Photocatalytic Property. *CrystEngComm*, 14: 4217-4222.

[31] Xue, C., Yan, X., An, H., Li, H., Wei, J., Yang, G. (2018). Bonding CdS-Sn_2S_3 Eutectic Clusters on Graphene Nanosheets with Unusually Photoreaction-driven Structural Reconfiguration Effect for Excellent H_2 Evolution and Cr(VI) Reduction. *Applied Catalysis B: Environmental*, 222: 157-166.

[32] Xin, X., Lang, J., Wang, T., Su, Y., Wang, X. (2016). Construction of Novel Ternary Component Photocatalyst $Sr_{0.25}H_{1.5}Ta_2O_6 \cdot H_2O$ Coupled with g-C_3N_4 and Ag Toward Efficient Visible Light Photocatalytic Activity for Environmental Remediation. *Applied Catalysis B: Environmental*, 181: 197-209.

[33] Deng, Y., Tang, L., Feng, C., Zeng, G., Wang, J., Zhou, Y., Liu, Y., Peng, B., Feng, H. (2018). Construction of Plasmonic Ag Modified Phosphorous-doped Ultrathin g-C_3N_4 Nanosheets/$BiVO_4$ Photocatalyst with Enhanced Visible-near-infrared Response Ability for Ciprofloxacin Degradation. *Journal of Hazardous Materials*, 344: 758-769.

[34] Chen, F., Yang, Q., Wang, Y., Yao, F., Ma, Y., Huang, X., Li, X., Wang, D., Zeng, G., Yu, H. (2018). Efficient Construction of Bismuth Vanadate-based Z-scheme Photocatalyst for Simultaneous Cr(VI) Reduction and Ciprofloxacin Oxidation under Visible Light: Kinetics, Degradation Pathways and Mechanism. *Chemical Engineering Journal*, 348: 157-170.

[35] Akpan, U.G., Hameed, B.H. (2009). Parameters Affecting the Photocatalytic Degradation of Dyes Using TiO_2-based Photocatalysts: A Review. *Journal of Hazardous Materials*, 170(2): 520-529.

[36] Djellabi, R., Ghorab, M.F. (2015). Photoreduction of Toxic Chromium Using TiO_2-immobilized under Natural Sunlight: Effects of Some Hole Scavengers and Process Parameters. *Desalination and Water Treatment*, 55: 1900-1907.

[37] Wang, X., Pehkonen, S.O., Ray, A.K. (2004). Removal of Aqueous Cr(VI) by a Combination of Photocatalytic Reduction and Coprecipitation. *Industrial & Engineering Chemistry Research*, 43: 1665-1672.

[38] Hao R., Wang G., Tang H., et al. (2016). Template-free Preparation of Macro/Mesoporous g-C_3N_4/TiO_2 Heterojunction Photocatalysts with Enhanced Visible Light Photocatalytic Activity [J]. *Applied Catalysis B: Environmental*, 187: 47-58.

[39] Kim, J., Lee, C., Choi, W. (2010). Platinized WO_3 as an Environmental Photocatalyst that Generates OH Radicals under Visible Light. *Environmental Science & Technology*, 44: 6849-6854.

[40] Hong, Y., Jiang, Y., Li, C., Fan, W., Yan, X., Yan, M., Shi, W. (2016). In-situ Synthesis of Direct Solid-state Z-scheme V_2O_5/g-C_3N_4 Heterojunctions with Enhanced Visible Light Efficiency in Photocatalytic Degradation of Pollutants. *Applied Catalysis B: Environmental*, 180: 663-673.